Empowering lithium-ion batteries

The potential of 2D o-Al2N2 as an exceptional anode material through DFT analysis

Agouri, M.; Benaddi, A.; Elomrani, A.; Khossossi, N.; Abbassi, A.; Hasnaoui, A.; Manaut, B.; Taj, S.; Driouich, M.

DOI
10.1016/j.est.2024.112351

Publication date
2024

Document Version
Final published version

Published in
Journal of Energy Storage

Journal of Energy Storage 94 (2024) 112351

Contents lists available at ScienceDirect

Journal of Energy Storage

journal homepage: www.elsevier.com/locate/est

Research papers

Empowering lithium-ion batteries: The potential of 2D o-Al_2N_2 as an exceptional anode material through DFT analysis

M. Agouri [a], A. Benaddi [b], A. Elomrani [b], N. Khossossi [c], A. Abbassi [a,*], A. Hasnaoui [b], B. Manaut [a], S. Taj [a], M. Driouich [a]

[a] Laboratory of Research in Physics and Engineering Sciences, Sultan Moulay Slimane University, Polydisciplinary Faculty, Beni Mellal, 23000, Morocco
[b] Sultan Moulay Slimane University, Polydisciplinary Faculty of Khouribga, LS2ME Laboratory, B.P. 145,25000 Khouribga, Morocco
[c] Department of Materials Science and Engineering, Faculty of Mechanical, Maritime and Materials Engineering, Delft University of Technology, Mekelweg 2, Delft, 2628 CD, The Netherlands

ARTICLE INFO

Keywords:
DFT
Two dimensional materials
o-Al_2N_2
Electrochemical properties
Lithium-ion battery

ABSTRACT

Finding an appropriate new anode material with high electrochemical performance for lithium-ion batteries (LIBs) is considered one of the significant challenges for both the academic and industrial research communities. Herein, we propose to explore the efficiency of a newly designed two-dimensional (2D) material, named orthorhombic dialuminium dinitride (o-Al_2N_2), as an alternative anode material for LIB systems through first-principles calculations and *ab initio* molecular dynamics (AIMD) simulations. The obtained results show that orthorhombic-Al_2N_2 exhibits a high specific capacity of 1144.2913 $mAhg^{-1}$, an operating voltage around 0.575 V, and a low kinetic diffusion barrier of 0.26 eV. These results prove the suitability of the o-Al_2N_2 monolayer as a promising anode material for LIBs with high structural stability, strong binding energy towards lithium adsorbent, fast lithium diffusion, and a high theoretical capacity. These features rank the 2D o-Al_2N_2 monolayer among the best choices for the anode part of the next-generation rechargeable LIBs.

1. Introduction

Scientists and researchers are currently making significant efforts to improve and develop effective energy storage strategies, which play an essential role in harnessing renewable and clean energies. These strategies have a crucial role in paving the way for the transition from fossil fuels and traditional energy sources to renewable energy [1,2]. In this regard, a secondary battery is the largest and most advanced energy storage technology owing to its diverse advantages, such as compact size, high energy density, and improved charge–discharge efficiency [3,4]. Specifically, rechargeable lithium-ion batteries (LIBs) have attracted significant attention from the research community, and they have been widely developed and incorporated into electronic devices and electric vehicles. [5–7]. Regrettably, conventional batteries have typically utilized graphite as the active electrode for the anode, exhibiting a low theoretical specific energy (250 Whkg) and a limited specific capacity of about 372 mAh/g [8]. However, these characteristics impose some limitations on meeting the growing demand for large-scale applications. In addition, several potential materials, such as germanium [9], silicon [10], carbon nanotube [11,12], and 2D blue and black phosphorene [13,14], have shown promise as anode materials with higher capacity compared to graphite. However, the instability and internal deformation of LIBs significantly impact battery life and safety. Hence, developing new advanced anode materials with high specific capacity, improved stability, and excellent cycle performance is a critical task for LIB applications.

Owing to several advantages, including a large surface-to-volume ratio, significant charge capacity, low diffusion barrier, and unique electronic and electrochemical properties, 2D materials have recently emerged as the most promising alternative for negative electrode material for LIBs [15–18]. To date, graphene stands out as the most well-known and extensively investigated material, mainly utilized as an anode material for LIBs [19,20]. Despite its amazing superlative properties, such as excellent structural stability and electrochemical performances, it is inactive to interact with Li-ion, leading to a low storage capacity [21,22]. In addressing this challenge, researchers have tried to overcome this problem by modifying the graphene structure through strategies such as doping and introducing extrinsic and intrinsic defects to improve and enhance Li-ion storage capacity. However, these modifications may degrade certain properties, such as conductivity and structural stability [23–26]. Then, researchers have intensively explored other two-dimensional materials with structures similar to

* Corresponding author.
E-mail addresses: abbassi.abder@gmail.com (A. Abbassi), b.manaut@usms.ma (B. Manaut).

https://doi.org/10.1016/j.est.2024.112351
Received 25 February 2024; Received in revised form 23 May 2024; Accepted 28 May 2024
Available online 10 June 2024

graphene, such as borophene [27], silicene [28], blue/black phosphorene [29,30], MXenes [31], transition metal dichalcogenides [32], and many others [33,34], which have been examined as anodes in LIB systems [35–37]. However, their utilization and application are generally limited, owing to their high diffusion energy barrier or low storage capacity [35]. For example, an alternative material that can be used as an anode is borophene, due to its significant specific storage capacity about of 1860 mAh/g with excellent stability.

To date, the III-V binary monolayer family is considered one of the most innovative classes of 2D materials for anode design in LIB systems due to their intriguing physical and chemical properties. Among these, hexagonal boron nitride monolayer (h-BN) has garnered significant attention, both theoretically and experimentally, owing to its potential applications in nanoelectronics. However, due to its large band gap energy (6.1 eV) and weak interaction with Li-ions, the h-BN monolayer is unsuitable for use as an active anode material in LIB systems [38,39]. Conversely, hexagonal h-BSb and h-BP have emerged as promising candidates for anode materials, boasting large theoretical specific capacities [40,41]. Furthermore, the hexagonal aluminum nitride monolayer (h-AlN) has been subject to theoretical investigation, demonstrating favorable properties for Li adsorption [42]. Sengupta [43] demonstrated that 2D h-AlN exhibits a high specific capacity of approximately 500.8 mAh/g with a low diffusion barrier, positioning h-AlN as a prospective material for anode applications in LIB systems. In 2021, J. Zhao et al. [44] proposed a novel 2D inorganic aluminum nitride material with an orthorhombic structure. Using density functional theory (DFT) investigations, they assessed its dynamic and mechanical stabilities. Optoelectronic properties revealed that the o-Al_2N_2 monolayer possesses semiconductor characteristics with an indirect band gap of approximately 0.941 eV (GGA-PBE approach) and exhibits high anisotropic optical absorbance, suggesting potential applications in clean energy technologies, including rechargeable batteries and hydrogen production. Importantly, the o-Al_2N_2 monolayer comprises aluminum and nitrogen elements, which are abundant and lightweight in nature, thus holding promise for achieving exceptional theoretical specific capacity in Li-ion batteries.

Motivated by the distinctive characteristics of orthorhombic Al_2N_2, as well as the successful synthesis of various 2D materials such as graphene and other 2D III-nitride materials [45], we aim to systematically explore, for the first time, the suitability of a 2D orthorhombic Al_2N_2 monolayer as a lithium-ion battery electrode using Density Functional Theory (DFT) calculations. We initially examined the structural stability and electronic properties of this material. Subsequently, the adsorption energy of lithium at favorable sites on the Al_2N_2 monolayer was investigated by incorporating DFT-D2 correction. Additionally, the mobility of lithium ions on the Al_2N_2 surface was evaluated across three different nearest neighboring sites using the climbing-image nudged-elastic-band (CI-NEB) method. Predictions for the theoretical capacity and open circuit voltage were made and analyzed in detail. We further confirmed the system's stability through *ab initio* molecular dynamics (AIMD) simulations. Our findings reveal that lithium adsorption induces a phase change in the host surface upon high ionic concentration. By calculating the average potential and specific capacity, we observed an exceptionally high capacity for lithium ions. In comparison with other 2D materials previously reported for anode applications, orthorhombic Al_2N_2 emerges as a promising anode material with a high specific capacity. Lastly, a comparative analysis with other recently predicted 2D materials for anode applications suggests that the proposed 2D Al_2N_2 monolayer stands out as one of the promising candidates for the anode component of lithium-ion battery (LIB) systems, showcasing both a high theoretical specific capacity and an ultralow diffusion barrier.

Table 1
The structural parameters of o-Al_2N_2 monolayer along with that of other monolayers build from binary elements in groups III and V for comparison.

Material	a (Å)	b (Å)	$d_{III-III}$	d_{III-V}	d_{V-V}
o-Al_2N_2	5.92	3.15	2.54	1.82	1.47
o-Al_2N_2 [44]	5.90	3.11	2.55	1.82	1.48
o-B_2N_2 [57]	4.57	2.50	1.70	1.44	1.44
o-B_2N_2 [44]	4.56	2.49	1.70	1.44	1.45
o-Ga_2N_2 [44]	5.80	3.17	2.39	1.87	1.44

2. Computational details

The structural stability, electronic, and electrochemical properties of the o-Al_2N_2 were investigated using the density functional theory [46] (DFT) as implemented in the Quantum Espresso (QE) code [47]. The exchange–correlation energy was described using the Perdew Burke Ernzerhof (PBE) functional within the generalized gradient approximation (GGA) [48]. The projected augmented wave (PAW) method was used to treat the electron–ion interactions [49]. The cutoff energy for the plane wave expansion is set to 884.37 Ry and the Brillouin zone was sampled using Monkhorst–Pack k-point meshes of $7 \times 11 \times 1$ and $11 \times 17 \times 1$ for the structural optimization and the electronic structure calculations [50]. For atomic relaxation, the energy and force convergences for self-consistency were set to 10^{-6} and 10^{-4} eV, respectively. The semi-empirical Grimme's (D2) approach was employed for taking into account the van der Waals interaction and describing accurately the interaction between the lithium-ion and o-Al_2N_2 surface [51]. A 20 Åvacuum along the z-axis was adopted to eliminate the interaction between the studied system and its periodic images. The charge transfer between the lithium atom and the monolayer was evaluated based-on the Bader charge algorithm [52]. We used both the XCrySDen and Vesta software for structural visualization [53,54]. The dynamical stability was investigated by calculating phonon dispersion along the high symmetry direction ($\Gamma - X - S - Y - \Gamma$) through density functional perturbation theory (DFPT) [55]. Climbing-image nudged-elastic-band (CI-NEB) [56] method was used to identify the minimum energy path and determine the activation energy barrier for the lithium diffusion on the surface of o-Al_2N_2 monolayer. Ab initio molecular dynamics (AIMD) simulations were conducted within the canonical ensemble framework (constant particle number, volume, and temperature, NVT), utilizing a timestep of 2 fs. To expedite the dynamical processes, a temperature of 300 K was employed. These AIMD simulations were instrumental in assessing the reversibility of observed structural changes and provided critical insights into the thermal stability of the host compound.

3. Results and discussion

3.1. Theoretical stability and electronic properties

Orthorhombic-Al_2N_2 (o-Al_2N_2) monolayer belongs to the aluminum nitride family, it is a planar structure with one atomic thick similar to that of graphene, h-AlN, and h-BN monolayers [19,42]. Fig. 1 shows the top and side views of the optimized structure of o-Al_2N_2 monolayer, where the unit cell is formed by four atoms (2Al and 2N). The optimized lattice parameters and bond lengths are listed in Table 1, along with those from other theoretical works. Notably, our theoretical findings entirely align with those reported in the literature, demonstrating the accuracy of the simulation method used in this work. The difference in bond lengths observed in comparison to other materials, such as o-B_2N_2 and o-Ga_2N_2 is referred to the difference in atomic radius between Al, Ga, and B.

While the experimental exploration of 2D materials is still in its nascent stages, theoretical stability assessments play a crucial role in advancing our understanding of these materials. For this purpose, we

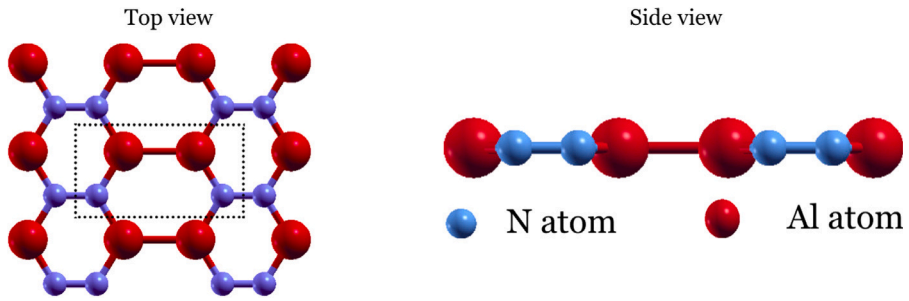

Fig. 1. Top and side views of a 3 × 2 × 1-supercell of the o-Al_2N_2 monolayer, where the unit cell is illustrated by the dotted rectangle. Blue and red spheres present the N and Al atoms, respectively. (For interpretation of the references to color in this figure legend, the reader is referred to the web version of this article.)

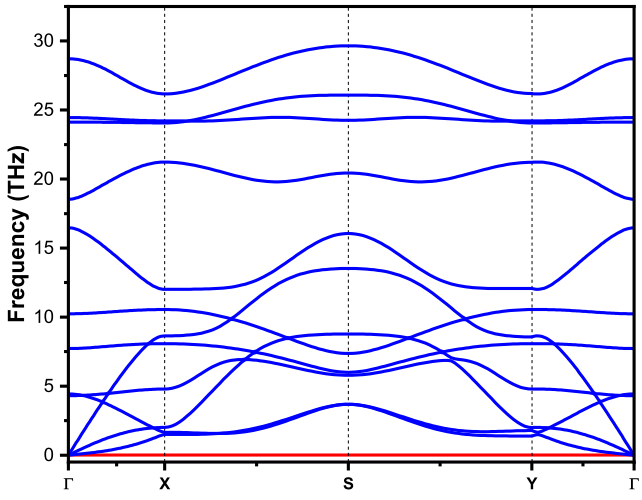

Fig. 2. The phonon dispersion curve of o-Al_2N_2 monolayer along high symmetry path $\Gamma - X - S - Y - \Gamma$.

estimated the theoretical stability of o-Al_2N_2 monolayer by calculating the cohesive energy and phonon dispersion curve which correspond respectively to the thermodynamic and dynamic stability. The cohesive energy per atom was calculated via the equation [58]:

$$E_c = \frac{E_{o-Al_2N_2} - 2(E_{Al} + E_N)}{4}, \quad (1)$$

where $E_{o-Al_2N_2}$ represents the total energy of o-Al_2N_2. E_{Al} and E_N are the total energies of isolated Al and N atoms, respectively. The calculated cohesive energy E_c is found to be −5.59 eV/atom, indicating a strong bonding network in o-Al_2N_2 monolayer. The value of cohesive energy is in the range of other 2D materials that have been experimentally and theoretically studied, like graphene (−7.9 eV), h-AlN (−5.36 eV/atom), silicene (−4.57 eV), phosphorene (−3.18 eV), and hexagonal boron–antimony (−4.48 eV) [40,59–62]. Additionally, we have compared the o-Al_2N_2 cohesive energy with other materials that have the same orthorhombic structure, such as o-B_2N_2 (−6.23 eV/atom) and o-B_2P_2 (−4.80 eV/atom) [63]. Additionally, we have checked the dynamical stability of the structure of o-Al_2N_2 monolayer through the phonon dispersion curve as depicted in Fig. 2. From this figure, there is no imaginary frequency mode throughout the high symmetry path along the first Brillouin zone (BZ), confirming the dynamical stability of the o-Al_2N_2 structure. Based on these results, we can conclude that 2D orthorhombic-Al_2N_2 is thermodynamically and dynamically stable which favors its experimental synthesis.

Fig. 3(a,b) presents the electronic band structure as well as the total/partial density of states (TDOS/PDOS) of the o-Al_2N_2 monolayer. The obtained electronic band structure depicts a semiconducting nature with an indirect band gap of 0.91 eV. The contribution of each atomic orbital to the conduction and valence bands can be analyzed from the TDOS and PDOS, as shown in Fig. 3(b). It can be observed that the conduction and valence bands are predominantly dominated by the p-orbitals of aluminum and nitride atoms. Near the Fermi level, a hybrid state between the p-orbitals of Al and N atoms could be observed. Moreover, it is evident that the observed opening gap in the electronic band structure essentially arises from the contribution and hybridization of the p-orbitals of N and Al atoms.

3.2. *Adsorption of single* (Li/Na/K) *atom*

Efficient anode materials for alkali-ion batteries hinge on the strong adsorption energy of alkali atoms onto the active surface, a fundamental criterion. Consequently, we undertook an investigation into the adsorption of alkali ions on a 3 × 2 × 1 supercell of the o-Al_2N_2 monolayer. Considering the symmetry of the o-Al_2N_2 monolayer, we initially identified seven potential sites, which can be categorized into three distinct categories: hollows (H), bridges (B), and tops (T), as delineated in Fig. 4. The hollows sites are denoted by H_1 and H_2, which correspond respectively, to Al_2N_4 and Al_4N_2 hexagons. The second class (bridge) contains B_1, B_2, and B_3 siting on Al-Al, N-N, and Al-N bonds, respectively, and the third class is the top (T) sitting on the top of each element Al and N atoms denoted by T_{Al} and T_N. The approach to recognize the outstanding binding site of alkali-ion on the o-Al_2N_2 monolayer is linked to the binding strength, which is given by its standard formula:

$$E_b = E_{A@Al_2N_2} - E_{o-Al_2N_2} - E_A \quad (2)$$

where $E_{A@Al_2N_2}$ and $E_{o-Al_2N_2}$ represent the total energies of the systems with and without lithium adsorption. E_A refers to the energy of a single alkali-ion in its bulk phase. As it is well-known, a higher negative binding strength corresponds to good stability of adatom in that binding configuration, leading to the fact that the adatoms can be distributed uniformly on the monolayer's surface instead of clustering. Consequentially, the issue of the formation of metal clusters is avoided during the charge/discharge process. Upon fully optimizing the o-Al_2N_2 system for the adsorption of Li, Na, and K at various active sites—namely, $H_{i=1,2}$, $B_{i=1,2,3}$, and $T_{Al,N}$ sites, we observed notable trends. Specifically, the H_1 and B_1 sites exhibited the lowest absorption energies, indicating their strong affinity for alkali metal adsorption. Further analysis revealed a shift in the preferred adsorption sites for all alkali metal atoms towards the hollow sites, with H_1 emerging as the most favorable site over B_1. The calculated binding energies for Li, Na, and K at the H_1 site were found to be −0.39, −0.23, and −0.17 eV, respectively. This can be explained based on a stronger interaction of lithium with the o-Al_2N_2 surface compared to sodium and potassium. Moreover, due to the larger atomic radii of Na and K compared to Li, structural deformations were observed upon their adsorption onto the o-Al_2N_2 surface. Such a results underscore the superior stability of Li ions when adsorbed on the o-Al_2N_2 monolayer, positioning it as a promising anode material for lithium-ion batteries. The estimated binding energies of Li at H_1 and B_1 sites (See Fig. 5(a,b)) were determined to be −0.39 eV

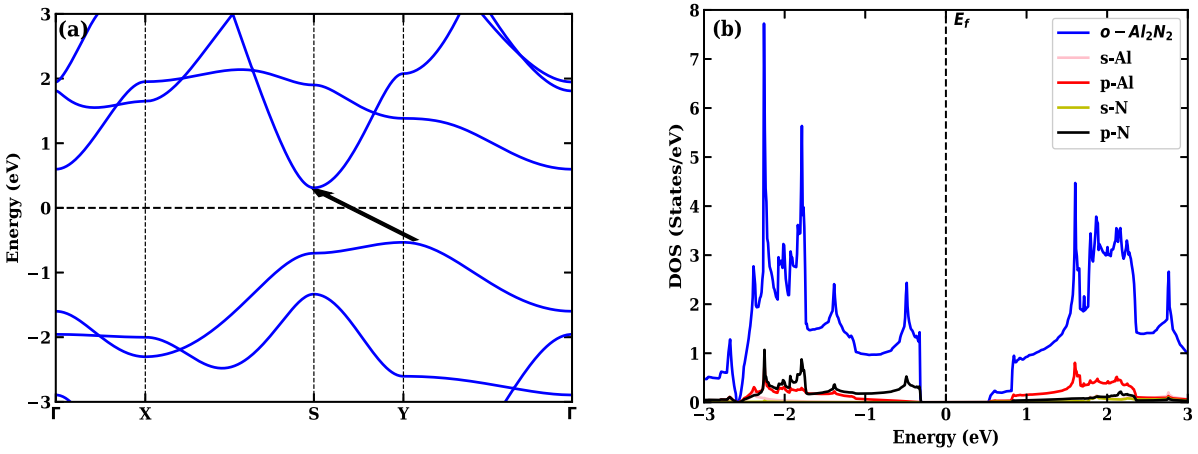

Fig. 3. Electronic band structure (a) and partial/total density of state (b) of the o-Al_2N_2 monolayer using PBE functional.

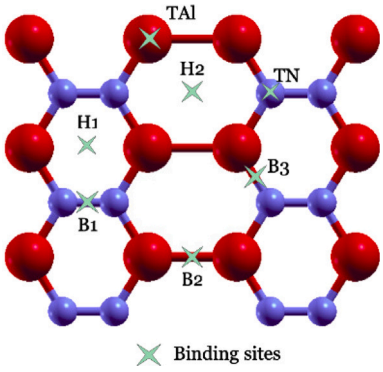

Fig. 4. The appropriate binding sites for alkali adsorption on supercell of o-Al_2N_2, where H_1 and H_2 refers to the hollow sites of the Al_2N_4 and Al_4N_2 hexagons, respectively. The B_1, B_2, and B_3 denote the binding sites at the N-N, Al-Al, and Al-N bonds, respectively. The T_N/T_{Al} presents the binding sites at the top of N/Al atom.

and −0.18 eV, respectively, with corresponding vertical distances of 1.55 Åand 1.93 Åbetween lithium and the monolayer surface. This suggests that the H_1 site is more favorable for Li adsorption. Additionally, the optimal coordination of lithium at sites H_1 and B_1 can be attributed to charge transfer mechanisms, wherein lithium readily transfers its valence charges to fill the vacant orbitals of aluminum atoms. It can be concluded that the o-Al_2N_2 monolayer exhibits superior stability and favorable adsorption characteristics for lithium compared to sodium and potassium. Therefore, our study advocates for the selective use of lithium as the preferred alkali metal for future applications involving o-Al_2N_2-based materials.

3.3. Charge density and Electronic conductivity

In order to understand and analyze the mechanism of interaction between lithium and the surface of o-Al_2N_2 during the insertion process, we calculate the charge density difference (CDD) of lithium-ion adsorbed at the optimal site on the orthorhombic-Al_2N_2 surface, using the following formula:

$$\Delta\rho = \rho_{Li@Al_2N_2} - \rho_{o-Al_2N_2} - \rho_{Li} \quad (3)$$

where $\rho_{Li@Al_2N_2}$ and $\rho_{o-Al_2N_2}$ correspond to the electronic charge density of the o-Al_2N_2 monolayer with and without one Li atom adsorbed, respectively, and the ρ_{Li} presents the electronic charge density of a single Li atom in an isolated system with the same cell volume. Fig. 6 represents the distribution of charge density by 3D iso-surface plot, revealing the accumulation and depletion of charge in our system. It can be noted that the charge accumulating and depleting zones are represented, respectively, by the yellow and blue colors, indicating an important charge transfer from Li to the o-Al_2N_2 monolayer. This significant charge transfer results from the higher electronegativity of Al and N atoms compared to the Li atom. The charge transfer, determined through the Bader charge analysis algorithm, was estimated to be 0.89 e. This indicates an oxidation process for lithium during its adsorption on the monolayer. Such behavior holds significant promise for energy storage applications. Moreover, to enhance the understanding of the interaction between a single lithium atom and the o-Al_2N_2 monolayer, we have computed its electronic properties. The electronic band structure, partial and total density of states for Li-adsorbed at the most favorable site H_1 on the o-Al_2N_2 surface are calculated, as shown in Fig. 7(a,b,c). Our results indicate that the studied system changes its electronic aspect from semiconductor to metallic nature after the adsorption of a single lithium atom. This change is illustrated by an overlap between valence and conduction bands leading to the shifting of the Fermi level towards the conduction band, as presented in band structure and total density of states (Fig. 7(a, b)). Similarly, the partial density of states curve (Fig. 7c) also shows that the Fermi level shifts to the conduction band, which validates the metallic aspect of the Li-adsorbed on the studied monolayer. This shift in the Fermi level corresponds to the p-orbits of Al/N atom and the contribution of s-orbital of a Li-atom, indicating a charge transfer from Li-adsorbed on the o-Al_2N_2 monolayer. These findings ensure significant electrical conductivity and a fast flow of electrons during the charge and discharge process [57].

3.4. Diffusion of Li-ion on o-Al_2N_2

The migration mechanism of lithium-ion on the o-Al_2N_2 nano-sheet is another key factor for exploiting and applying this 2D material as an efficient anode material in LIB systems. In fact, the rate performance of the charge/discharge process in LIB systems is related to the movement of Li-ions in the active materials. In this regard, the mobility of Li-ion on the o-Al_2N_2 surface can be analyzed by calculating the diffusion energy barrier of lithium. Using the climbing image nudged elastic band (CI-NEB) method, we calculated the diffusion energy barrier by investigating the minimum energy path and finding the saddle point along the paths, where lithium migrates from the most favorable to its neighbor. The available diffusion pathways for Li-ion on o-Al_2N_2 monolayer are shown in Fig. 8(a,b,c). Three possible migration pathways are considered: the first one (Fig. 8a) goes along the x-direction (zigzag), the second one (Fig. 8b) follows along the y-direction passing on the top of the Al atom, and the third (Fig. 8c) passes above the H_2 sites. Fig. 8 illustrate a representation of the three pathways along with their energy profiles. From the energy difference between the minimum and

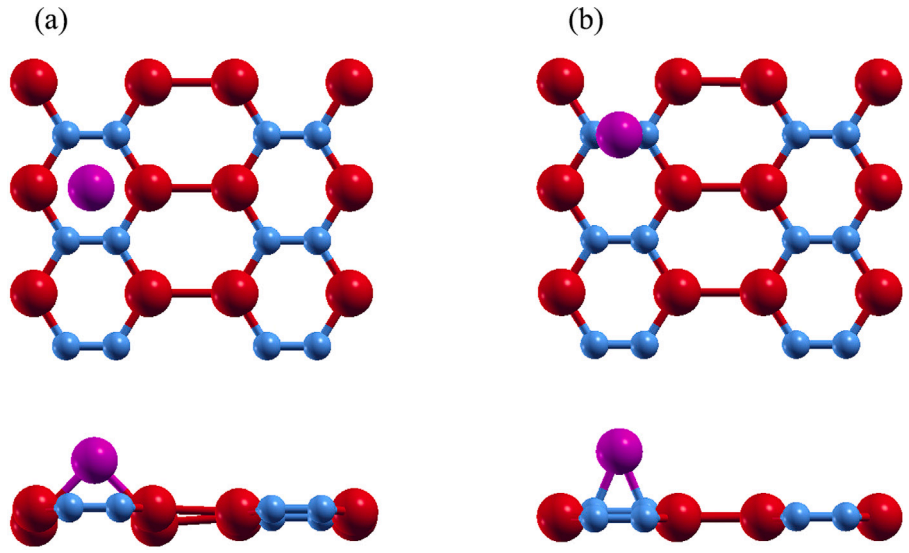

Fig. 5. Top and side views of the optimized structures of lithium (pink atom) adsorbed on o-Al_2N_2 monolayer at (a) H_1-site and (b) B_1-site. (For interpretation of the references to color in this figure legend, the reader is referred to the web version of this article.)

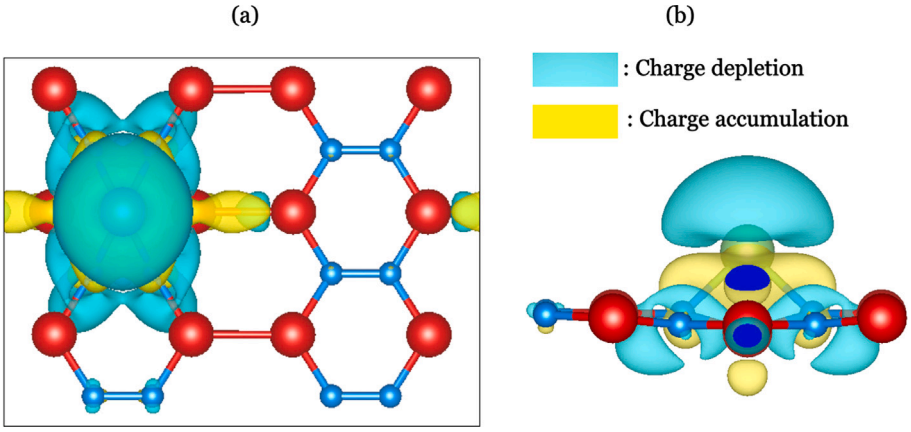

Fig. 6. Top (a) and side (b) views of the charge density difference ($\Delta\rho$) for Li-ion adsorbed at the most stable binding site (H_1) on o-Al_2N_2 monolayer. The accumulation and depletion of electrons are indicated, respectively, by the yellow and blue colors, and the charge transfer from the Li-atom to the o-Al_2N_2 surface is about 0.89 e. (For interpretation of the references to color in this figure legend, the reader is referred to the web version of this article.)

saddle points, the obtained diffusion barrier heights of Li-ion along the paths-a, b, and c are, respectively, 0.26, 0.65, and 0.70 eV. Resulting in lithium diffusion along path-a is the most favorable with a small energy barrier of 0.26 eV. The orthorhombic-Al_2N_2 monolayer presents a significant energy barrier (0.26 eV), which is small compared to other 2D materials like h-BAs monolayer (0.52 eV), h-AlN monolayer (0.40 eV), and o-B_2N_2 monolayer (0.38 eV) [43,57,64].

3.5. Open circuit voltage and theoretical capacity

The theoretical specific capacity and the open circuit voltage (OCV) are another two crucial factors that influence the performance of batteries. To simulate the lithium loading process, we incrementally increased the number of lithium adatoms by filling the most favorable sites (H_1-sites) on both sides of the monolayer of o-Al_2N_2, adding one adatom at a time until a complete recovery was achieved, forming the first layer of Li ($Li_6Al_2N_2$). Subsequently, Li atoms were added into the second favorable sites at B_1-sites, creating the second layer ($Li_{12}Al_2N_2$). Therefore, a series of intermediate configurations under the chemical formula of $Li_nAl_2N_2$ (where n = 6, 12, 18, 24, 30, 36, 42) are considered, as presented in Fig. 9. Accordingly, the average adsorption energy E_b^{avg} of Li atoms adsorbed on o-Al_2N_2 surface is calculated using the following formula :

$$E_b^{avg} = \frac{E_{Li_n@Al_2N_2} - E_{o-Al_2N_2} - nE_{Li}}{n} \quad (4)$$

where $E_{Li_n@Al_2N_2}$ and $E_{o-Al_2N_2}$ represent the ground state energies of $Li_n@Al_2N_2$ and o-Al_2N_2, respectively. E_{Li} refers to the energy of a single lithium-ion in the bcc phase. The insertion process continues until the average adsorption energy becomes positive, which is a strong indication of the beginning of Li clustering formation and dendrites. The E_b^{avg} for layer 1, layer 2, layer 3, layer 4, layer 5, layer 6, and layer 7 are found to be −0.21, −0.67, −0.29, −0.15, −0.09, −0.0135, and −0.0137 eV, respectively. As a result, the orthorhombic-Al_2N_2 anode for lithium-ion batteries could store a maximum of 42 Li-atoms, where the average adsorption energy approach zero.

The open-circuit voltage (OCV) is a significant parameter that aids in understanding the electrochemical behavior and the applicability of anode materials and their performance in rechargeable lithium-ion batteries. The Nernst equation for determining OCV is expressed as :

$$V = \frac{-\Delta G}{nF} \quad (5)$$

where F, ΔG, and n present the Faraday constant, the change in Gibbs free energy, and number of transferred charge, respectively. In solid

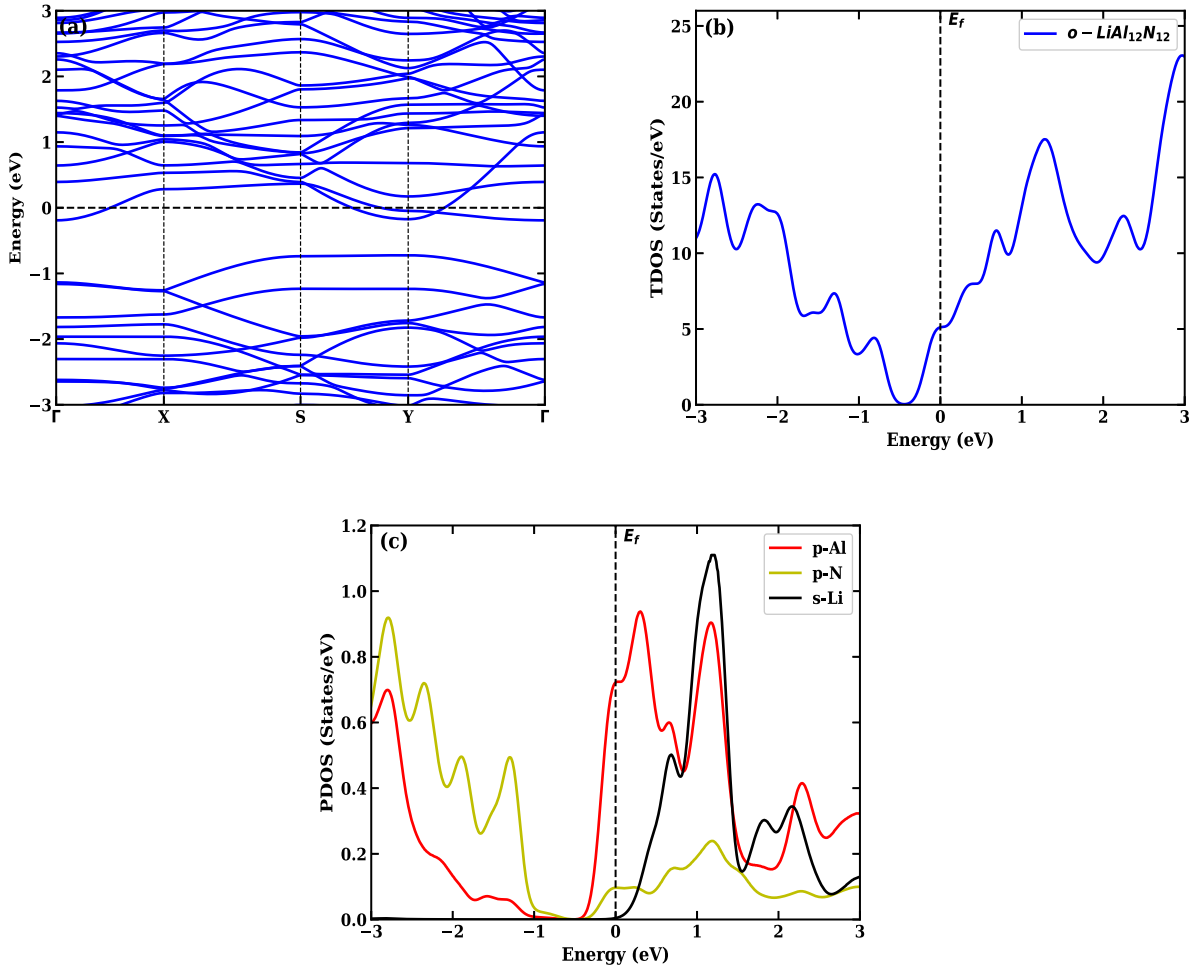

Fig. 7. Electronic band structure (a), total density of states (b), and partial density of states (c) curves of a single Li-adsorbed on o-Al_2N_2 monolayer.

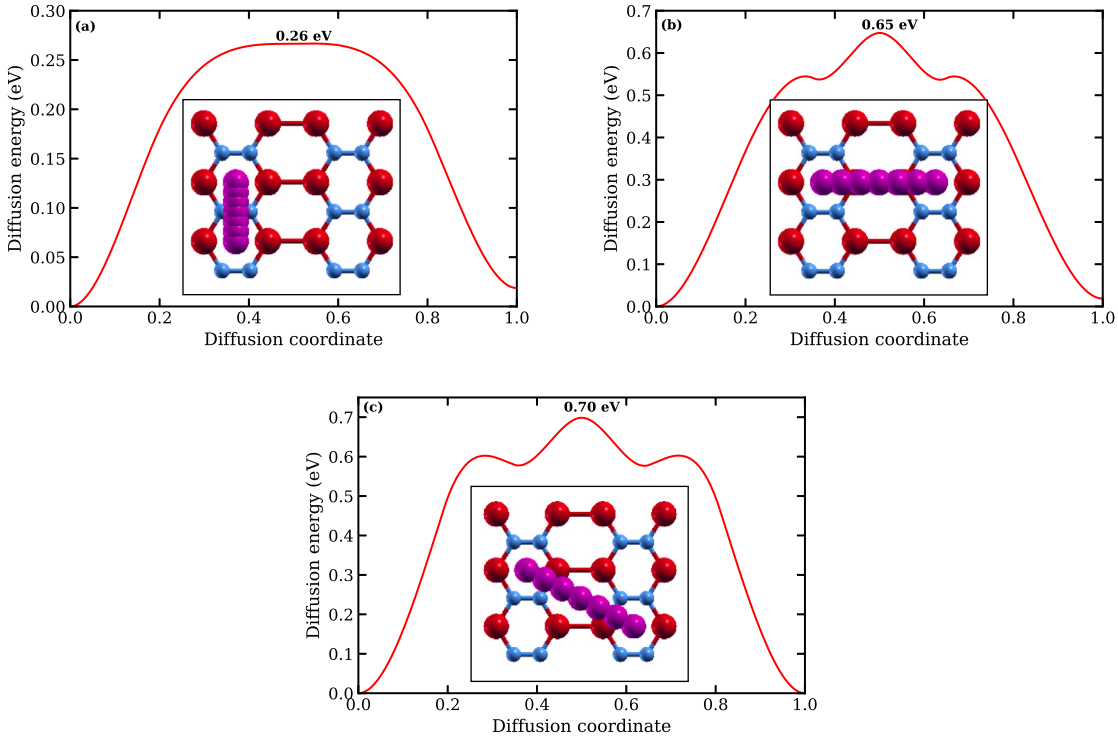

Fig. 8. The diffusion pathways and their energy profiles for lithium-ion diffusion on the surface of o-Al_2N_2 monolayer.

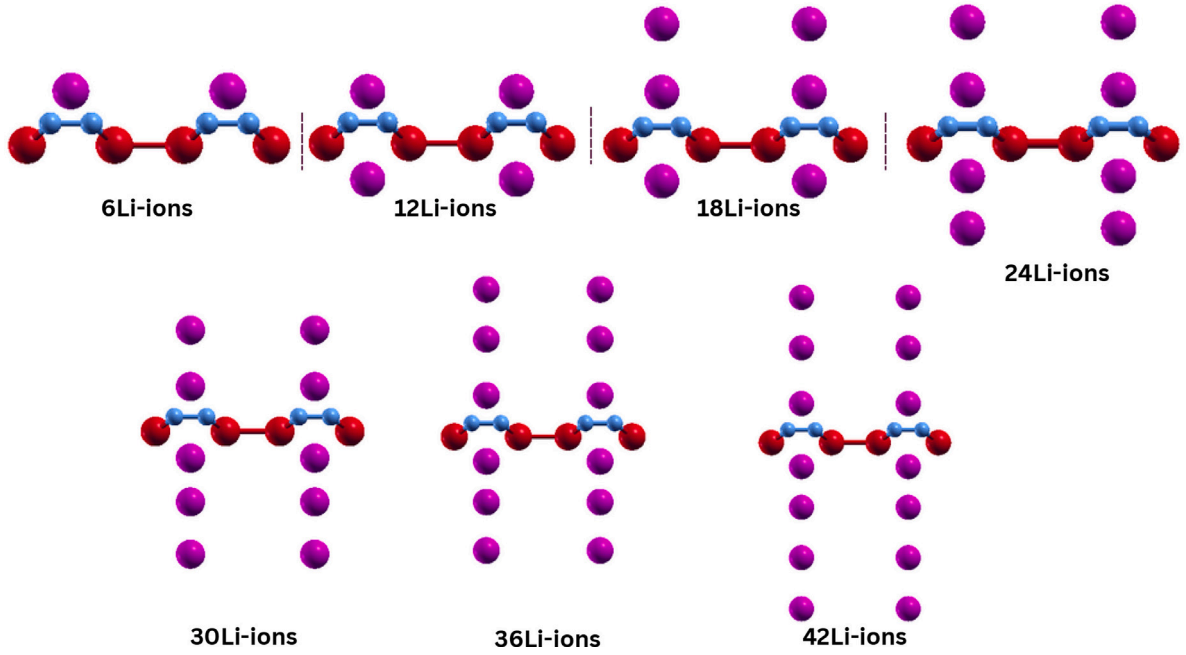

Fig. 9. Structural side view of different Li-adsorbed concentrations on o-Al_2N_2 monolayer.

state case, the contributions of volume change, entropy, and pressure are neglected, the open circuit voltage (OCV) leads to:

$$OCV = \frac{-E_{\mathrm{Li}_{n_2}@\mathrm{Al_2N_2}} + E_{\mathrm{Li}_{n_1}@\mathrm{Al_2N_2}} + (n_2 - n_1)E_{\mathrm{Li}}}{e(n_2 - n_1)} \tag{6}$$

where $E_{\mathrm{Li}_{n_2}@\mathrm{Al_2N_2}}$ and $E_{\mathrm{Li}_{n_1}@\mathrm{Al_2N_2}}$ are the energy at n_2 and n_1 number of Li-adsorbed on the 2D o-Al_2N_2, and e is the electronic charge. For an accurate OCV profile, the formation energy was calculated first for all the considered concentrations of lithium adatoms in order to get the convex minimum energy hull which is plotted using following equation:

$$E_f = E_{\mathrm{Li}_n@\mathrm{Al_2N_2}} - \left\{ \frac{nE_{\mathrm{Li}_{n_{max}}@\mathrm{Al_2N_2}} + (n_{max} - n)E_{o-\mathrm{Al_2N_2}}}{n_{max}} \right\} \tag{7}$$

where $E_{\mathrm{Li}_n@\mathrm{Al_2N_2}}$ and $E_{\mathrm{Li}_{n_{max}}@\mathrm{Al_2N_2}}$ are the total energy for n lithium atoms and total energy of maximum Li loaded o-Al_2N_2, respectively. Fig. 10(a) shows the formation energy as a function of the number of Li-atoms adsorbed. From the convex hull plot, we observe only one stable intermediate structure for $n = 12$ Li-atoms. Furthermore, the remaining configurations are considered as meta-stable, and they are not included in the OCV calculation. The corresponding result of the OCV profile of our system as a function of the number of Li-adsorbed is illustrated in Fig. 10(b). We can see that the average OCV curve presents a small positive values less than 1.5 V, confirming the suitability of the o-Al_2N_2 monolayer as a negative electrode for lithium ion batteries. The observed trend for OCV profile and average adsorption energy is a consequence of the strengthening repulsive interactions between lithium ions, which intensify with the increasing number of lithium adatoms. Furthermore, with higher than 42 Li-adatoms, the OCV profile shows a change from the positive to negative value, indicating that the Li-atoms have reached the maximum adsorption number on the o-Al_2N_2 monolayer. The average OCV of our system is approximately 0.575 V, which within an ideal range for achieving maximum power density during the charging/discharging. Consequently, the o-Al_2N_2 monolayer has a potential to serve as a high performance prospective anode for LIBs. Based on these results, the theoretical specific capacity (C) of o-Al_2N_2 as an anode material for lithium-storage can be computed by the formula:

$$C = \frac{n_{max}.F}{M_{o-\mathrm{Al_2N_2}}} \tag{8}$$

where $M_{o-\mathrm{Al_2N_2}}$ refers to the relative molecular mass of o-Al_2N_2 monolayer. n_{max} and F present the maximum number of Li-adsorbed, and Faraday constant. According to the maximum number of Li-atoms stored on the orthorhombic-Al_2N_2 surface, the theoretical specific capacity is about 1144.2913 $mAhg^{-1}$. This capacity is higher than that of many 2D materials such as graphite [19], h-BSb [40] and h-AlN [43], which makes o-Al_2N_2 a promising candidate for the next generation LIB systems.

In addition, the change in cell volume during charging/discharging process of an electrode material can impact the cycle life of batteries. For this reason, we have assessed the changing volume by calculating the ratio of the change in volume of the o-Al_2N_2 monolayer. The result exhibits a small shrinking in the cell volume, approximately 2.87% at maximum storage, indicating excellent cycling performances of the monolayer. The obtained change in volume is small compared to the commercial anode material graphite [65], and recently predicted 2D anode materials such as SiP_3, WB_4, Si_3C, and FeSe [66–69].

Furthermore, it is highly intriguing to note the remarkably high storage capacity of the o-Al_2N_2 monolayer compared to previously reported anode materials for LIBs. Fig. 11 illustrates the obtained results for storage capacity and diffusion barrier, comparing them with those of some typical 2D anode materials for Li-ion batteries [64,70–78]. Firstly, the achieved storage capacity of the o-Al_2N_2 material surpasses that of the commercial graphite anode material by approximately four times. Moreover, it is evident that the obtained storage capacity of the o-Al_2N_2 material is higher than that of other anode materials reported in the literature, such as h-AlC, silicene, α-CP, and many more. However, it is lower compared to other materials, including o-B_2P_2, Siliborophene, VSi_2N_4, and TiC_3 [79–82]. Additionally, the o-Al_2N_2 monolayer exhibits a significantly low diffusion barrier compared to certain reported anode materials, particularly to the o-B_2P_2 monolayer. This ensures excellent mobility of Li-ions on the surface, facilitating the smooth operation of lithium-ion battery systems. Finally, the orthorhombic Al_2N_2 material in the comparison plot highlights its advantages and potential as a promising anode material, characterized by an ultra-low diffusion barrier and high storage capacity.

3.6. *Further insights into the stability of o-*Al_2N_2 *during lithiation processes*

During the charge–discharge process, the battery electrode materials can undergo significant volume expansion, potentially leading to

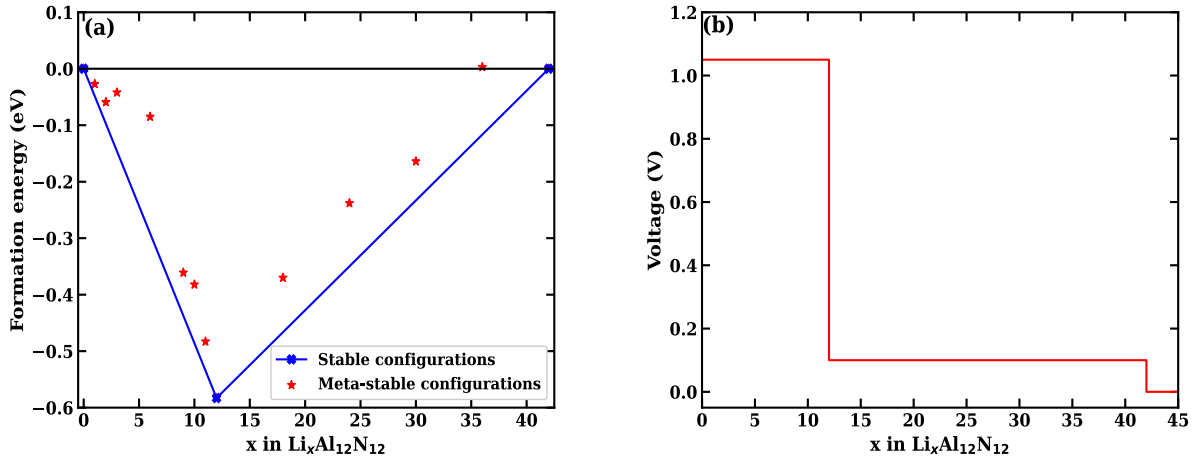

Fig. 10. The formation energy of $Li_xAl_{12}N_{12}$ per formula unit (a) and the estimated OCV profile as a function of numbers x for $Li_xAl_{12}N_{12}$ (b).

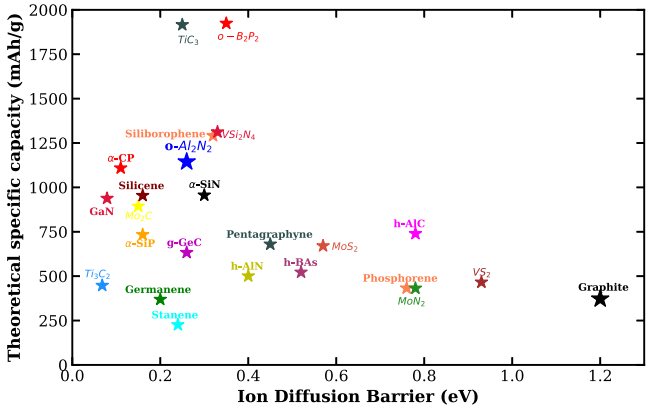

Fig. 11. A Comparison of the theoretical specific capacity (C) and diffusion energy barrier of o-Al_2N_2 monolayer with other previously potential 2D anode materials.

their pulverization. This phenomenon may result in a sharp decline in specific capacity and diminished battery cycle life. In this context, both mechanical and thermal stability of o-Al_2N_2 anode material during lithiation were investigated. The elastic characteristics of the o-Al_2N_2 monolayer before and after a single Li-insertion were analyzed using the energy–strain approach based on the stiffness tensor from the second-order derivative of the total energy relative to the applied tensile and compressive strains ranging from −1.5% to +1.5% in increments of 0.50%. The elastic strain energy per unit area is quantified using the Voigt notation and is represented by the following formula:

$$U(\epsilon_x, \epsilon_y) = \frac{1}{2}C_{11}\epsilon_x^2 + \frac{1}{2}C_{22}\epsilon_y^2 + C_{12}\epsilon_x\epsilon_y \tag{9}$$

where ϵ_x and ϵ_y representing uniaxial strains along the x- and z-directions respectively, the elastic constants C_{11} and C_{22} differ due to the anisotropic nature of the o-Al_2N_2 monolayer.

The calculated elastic constants meet the established criteria for mechanical stability, which require $C_{11} > 0$, $C_{22} > 0$, $C_{66} > 0$, and $C_{11}.C_{22} - C_{12}^2 > 0$. As detailed in Table 2, the C_{11} = 148.43 N/m, C_{12} = 28.59 N/m, C_{22} = 146.87 N/m, and C_{66} = 46.55 N/m, which are slightly comparable to those of o-B_2P_2 and significantly smaller than those of h-AlN and o-B_2N_2. Additionally, the mechanical properties are quantified by the in-plane Young's modulus and the Poisson's ratio along the x- and y-directions, computed using the respective formulas:

$$Y_x = \frac{C_{11}C_{22} - C_{12}C_{21}}{C_{22}}, \quad Y_y = \frac{C_{11}C_{22} - C_{12}C_{21}}{C_{11}} \tag{10}$$

Table 2
A comparative analysis of the elastic constants (C_{11}, C_{12}, C_{22}, and C_{66}) derived for various 2D materials.

2D materials	Elastic constants (N/m)			
	C_{11}	C_{12}	C_{22}	C_{66}
o-Al_2N_2	148.43	28.59	146.87	46.55
Al_2N_2@Li	145.12	28.59	143.80	44.38
o-B_2P_2 [83]	154.4	34.7	135.7	49.6
o-B_2N_2 [57]	250.39	35.11	291.65	21.98
h-AlN [84]	182.48	88.29	173.85	94.35

$$v_x = \frac{C_{12}}{C_{22}}, \quad v_y = \frac{C_{12}}{C_{11}} \tag{11}$$

The calculated in-plane Young's modulus in the x- and y-direction are about 143 N/m and 141 N/m, respectively. While the Poisson's ratio is calculated to be v_x = 0.194 and v_y = 0.192. As compared to some other 2D materials, these results are slightly greater than h-AlN, and o-B_2P_2 monolayers [83,84], while they are smaller than those of the o-B_2N_2 monolayer [57].

The thermal stability was further confirmed through *ab initio* molecular dynamics (AIMD) simulations. As indicated earlier, the optimal lithium concentration was established based on two principal factors: the necessity for the average adsorption energy to be negative and maintaining the electrode's thermal stability throughout the charge/discharge cycles. It is crucial to emphasize the observed structural changes with lithium insertion, depicted in Fig. 9. Initially, the system retains its structure with minor lithium intercalation, but exhibits buckling at higher concentrations. This buckling is caused by additional electrons from lithium atoms, which compromise the stability of the orthorhombic Al_2N_2 surface. Corresponding AIMD simulations, conducted over 10 ps at 300 K, were utilized to evaluate the o-Al_2N_2 anode's recovery dynamics, as shown in Fig. 12. The minimal variation in total energy across this MD timescale underscores the exceptional thermal stability of $Li_7Al_2N_2$. Following these simulations, lithium atoms were extracted from the o-Al_2N_2 surface, and a subsequent AIMD as well as a global energy optimization confirmed the structure's reversibility, returning it to its original planar phase.

4. Conclusion

In conclusion, the proposed 2D o-Al_2N_2 monolayer has been theoretically investigated as an anode material in lithium-ion battery systems through DFT calculations. The negative cohesive energy and the absence of negative frequencies in the phonon dispersion indicate the theoretical stability of orthorhombic-Al_2N_2 material. The binding

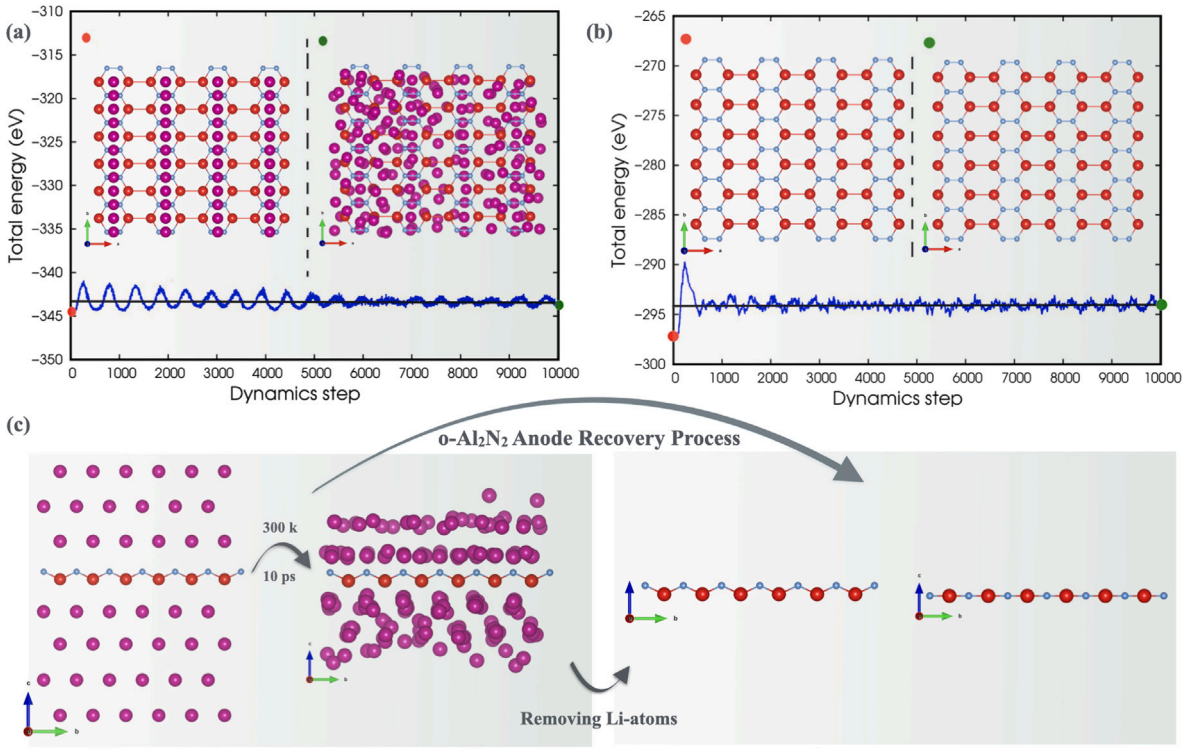

Fig. 12. The o-Al_2N_2 battery anode recovery process with fully removed Li-ions by AIMD at 300 K and a time scale 10 ps.

strength of lithium at the most stable site (Al_2N_4 hollow) is strong, with a value of approximately −0.39 eV, primarily due to charge transfer from lithium to the *o*-Al_2N_2 monolayer (0.89 e), which is desirable for anode material as it avoids the cluster formation of lithium during the intercalation process. Throughout the storage process, the *o*-Al_2N_2 monolayer demonstrates a favorable average voltage of about 0.575 V and a high storage capacity of 1144.2913 mAh/g, significantly greater than that of the commercial graphite anode. Moreover, the *o*-Al_2N_2 monolayer facilitates the rapid mobility of Li atoms, with an ultra-low energy barrier of 0.26 eV. Furthermore, a small volume shrinkage (approximately ∼ 2.87%) is observed, indicating the excellent cycling performance of our suggested material. Based on our findings, the 2D *o*-Al_2N_2 monolayer emerges as a novel and promising candidate for anode material in LIBs.

CRediT authorship contribution statement

M. Agouri: Writing – original draft, Software, Conceptualization. **A. Benaddi:** Writing – original draft, Data curation, Conceptualization. **A. Elomrani:** Writing – original draft, Software, Conceptualization. **N. Khossossi:** Writing – review & editing, Software, Investigation. **A. Abbassi:** Writing – review & editing, Supervision, Investigation. **A. Hasnaoui:** Supervision. **B. Manaut:** Supervision. **S. Taj:** Visualization, Validation, Supervision. **M. Driouich:** Validation, Supervision.

Declaration of competing interest

The authors declare that they have no known competing financial interests or personal relationships that could have appeared to influence the work reported in this paper.

Data availability

Data will be made available on request.

Acknowledgments

This research was performed using computational resources of HPC-MARWAN (www.marwan.ma/hpc) provided by the National Center for Scientific and Technical Research (CNRST), Rabat, Morocco.

References

[1] Y. Sun, N. Liu, Y. Cui, Nat Energy 1 (2016) 616–620, http://dx.doi.org/10.1038/nenergy.2016.71.
[2] X.B. Cheng, R. Zhang, C.Z. Zhao, Q. Zhang, Chem. Rev. 117 (2017) 10403–10473, http://dx.doi.org/10.1021/acs.chemrev.7b00115.
[3] J.B. Goodenough, Y. Kim, Chem. Mater. 22 (2010) 587–603, http://dx.doi.org/10.1021/cm901452z.
[4] J.B. Goodenough, K.S. Park, J. Am. Chem. Soc. 135 (2013) 1167–1176, http://dx.doi.org/10.1021/ja3091438.
[5] J. Duan, et al., Electrochem. Energ. Rev. 3 (2020) 1–42, http://dx.doi.org/10.1007/s41918-019-00060-4.
[6] Y. Hua, et al., Resour. Conserv. Recycl. 168 (2021) 105249, http://dx.doi.org/10.1016/j.resconrec.2020.105249.
[7] B. Dunn, H. Kamath, J.M. Tarascon, Science 334 (2021) 928–935, http://dx.doi.org/10.1126/science.1212741.
[8] J.R. Dahn, T. Zheng, Y. Liu, J.S. Xue, Science 270 (1995) 590–593, http://dx.doi.org/10.1126/science.270.5236.590.
[9] C.K. Chan, X.F. Zhang, Y. Cui, Nano Lett. 8 (2008) 307–309, http://dx.doi.org/10.1021/nl0727157.
[10] G.A. Tritsaris, et al., Nano Lett. 13 (2013) 2258–2263, http://dx.doi.org/10.1021/nl400830u.
[11] E. Frackowiak, et al., Carbon 37 (1999) 61–69, http://dx.doi.org/10.1016/S0008-6223(98)00187-0.
[12] E. Frackowiak, et al., Phys. Rev. Lett. 88 (2002) 015502, http://dx.doi.org/10.1103/PhysRevLett.88.015502.
[13] J. Cheng, et al., Nano-Micro Lett. 12 (2020) 38, http://dx.doi.org/10.1007/s40820-020-00510-5.
[14] Q. Li, et al., Phys. Chem. C 119 (2015) 8662–8670, http://dx.doi.org/10.1021/jp512411g.
[15] Z. Zhang, et al., Chem. Mater. 30 (2018) 3208–3214, http://dx.doi.org/10.1021/acs.chemmater.7b05311.
[16] D. Das, et al., Phys. Chem. Chem. Phys. 19 (2017) 24230, http://dx.doi.org/10.1039/c7cp04451h.
[17] J. Rehman, et al., Appl. Surf. Sci. 496 (2019) 143625, http://dx.doi.org/10.1016/j.apsusc.2019.143625.

[18] Lixin Xiong, et al., Phys. Chem. Chem. Phys. 21 (2019) 7053–7060, http://dx.doi.org/10.1039/C8CP07398H.
[19] J. Zheng, et al., Appl. Surf. Sci. 258 (2011) 1651–1655, http://dx.doi.org/10.1016/j.apsusc.2011.09.007.
[20] M.R. Al Hassan, et al., Mater. Today Chem. 11 (2019) 225–243, http://dx.doi.org/10.1016/j.mtchem.2018.11.006.
[21] M. Liu, et al., J. Phys. Chem. Lett. 5 (2014) 1225–1229, http://dx.doi.org/10.1021/jz500199d.
[22] Z. Du, et al., Mater. Chem. A (2014) 9164–9168, http://dx.doi.org/10.1039/c4ta00345d.
[23] H. Yildirim, et al., ACS Appl. Mater. Interfaces 6 (2014) 21141–21150, http://dx.doi.org/10.1021/am506008w.
[24] Z.S. Wu, et al., ACS Nano 5 (2011) 5463–5471, http://dx.doi.org/10.1021/nn2006249.
[25] X. Fan, et al., ACS Appl. Mater. Interfaces 4 (2012) 2432–2438, http://dx.doi.org/10.1021/am3000962.
[26] X. Zhao, et al., ACS Nano 5 (2011) 8739–8749, http://dx.doi.org/10.1021/nn202710s.
[27] B. Mortazavi, et al., J. Power Sources 329 (2016) 456–461, http://dx.doi.org/10.1016/j.jpowsour.2016.08.109.
[28] J. Zhuang, et al., Adv. Mater. 29 (2017) 1606716, http://dx.doi.org/10.1002/adma.201606716.
[29] J. Zhu, et al., Nano-Micro Lett. 12 (2020) 120, http://dx.doi.org/10.1007/s40820-020-00453-x.
[30] Q. Li, et al., J. Phys. Chem. C 119 (2015) 8662–8670, http://dx.doi.org/10.1021/jp512411g.
[31] S. Sun, et al., J. Chem. Eng. 338 (2018) 27–45, http://dx.doi.org/10.1016/j.cej.2017.12.155.
[32] X. Sun, et al., Beilstein J. Nanotechnol. 8 (2017) 2711–2718, http://dx.doi.org/10.3762/bjnano.8.270.
[33] N. Khossossi, et al., J. Power Sources 485 (2021) 229318, http://dx.doi.org/10.1016/j.jpowsour.2020.229318.
[34] A. Hosseinian, et al., J. Mol. Model. 23 (2017) 354, http://dx.doi.org/10.1007/s00894-017-3527-1.
[35] P.U. Nzereogu, et al., Appl. Surf. Sci. 9 (2022) 100233, http://dx.doi.org/10.1016/j.apsadv.2022.100233.
[36] S. Zhao, et al., J. Mater. Chem. A 2 (2014) 19046, http://dx.doi.org/10.1039/C4TA04368E.
[37] B. Mortazavi, et al., Electrochim. Acta 213 (2016) 865–870, http://dx.doi.org/10.1016/j.electacta.2016.08.027.
[38] H. Sahin, et al., Phys. Rev. B 80 (2009) 155453, http://dx.doi.org/10.1103/PhysRevB.80.155453.
[39] L. Song, et al., Nano Lett. 10 (2010) 3209–3215, http://dx.doi.org/10.1021/nl1022139.
[40] A. Elomrani, et al., Mater. Chem. Phys. 275 (2022) 125191, http://dx.doi.org/10.1016/j.matchemphys.2021.125191.
[41] S. Ullah, et al., ACS Omega 3 (2018) 16416–16423, http://dx.doi.org/10.1021/acsomega.8b0260.
[42] C. Bacaksiz, et al., Phys. Rev. B 91 (2015) 085430, http://dx.doi.org/10.1103/PhysRevB.91.085430.
[43] A. Sengupta, Appl. Surf. Sci. 451 (2018) 141–147, http://dx.doi.org/10.1016/j.apsusc.2018.04.264.
[44] J. Zhao, et al., Phys. Chem. Chem. Phys. 32 (2021) 3771, http://dx.doi.org/10.1039/d0cp05909a.
[45] J. Ben, et al., Adv. Mater. 33 (2021) e2006761, http://dx.doi.org/10.1002/adma.202006761.
[46] E.K.U. Gross, et al., Density Functional Theory, 1993, http://dx.doi.org/10.1007/978-1-4757-9975-0.
[47] P. Giannozzi, et al., J. Phys.: Condens. Matter. 29 (2017) 465901, http://dx.doi.org/10.1088/1361-648X/aa8f79.
[48] J. Paier, J. Chem. Phys. 23 (2005) 234102, http://dx.doi.org/10.1063/1.1926272.
[49] P.E. Blöchl, Phys. Rev. B 50 (1994) 17953, http://dx.doi.org/10.1103/PhysRevB.50.17953.
[50] H.J. Monkhorst, et al., Phys. Rev. B 13 (1976) 5188, http://dx.doi.org/10.1103/PhysRevB.13.5188.
[51] S. Grimme, J. Comput. Chem. 27 (2006) 1787–1799, http://dx.doi.org/10.1002/jcc.20495.
[52] G. Henkelman, et al., Comput. Mater. Sci. 36 (2006) 354–360, http://dx.doi.org/10.1016/j.commatsci.2005.04.010.
[53] K. Momma, et al., J. Appl. Crystallogr. 44 (2011) 1272–1276, http://dx.doi.org/10.1107/S0021889811038970.
[54] A. Kokalj, Comp. Mater. Sci. 28 (2003) 155–168, http://dx.doi.org/10.1016/S0927-0256(03)00104-6.
[55] X. Gonze, Phys. Rev. A 54 (1996) 4591, http://dx.doi.org/10.1103/PhysRevA.52.1096.
[56] G. Henkelman, et al., J. Chem. Phys. 113 (2000) 9901–9904, http://dx.doi.org/10.1063/1.1329672.
[57] N. Khossossi, et al., Nano Energy 96 (2022) 107066, http://dx.doi.org/10.1016/j.nanoen.2022.107066.
[58] Q. He, et al., Energy Environ. Mater. (2019) 1–16, http://dx.doi.org/10.1002/eem2.12056.
[59] W. Hu, et al., J. Phys. Chem. C 119 (2015) 20474–20480, http://dx.doi.org/10.1021/acs.jpcc.5b06077.
[60] E.F. de Almeida, et al., Eur. Phys. J. B 85 (2012) 48, http://dx.doi.org/10.1140/epjb/e2011-20538-6.
[61] N.D. Drummond, et al., Phys. Rev. B 85 (2012) 075423, http://dx.doi.org/10.1103/PhysRevB.85.075423.
[62] T. Frank, et al., Phys. Rev. X 9 (2019) 011018, http://dx.doi.org/10.1103/PhysRevX.9.011018.
[63] A. Benaddi, et al., Sustain. Energy Fuels 8 (2024) 1719–1729, http://dx.doi.org/10.1039/D4SE00173G.
[64] N. Khossossi, et al., Phys. Chem. Chem. Phys. 21 (2019) 18328–18337, http://dx.doi.org/10.1039/C9CP03242H.
[65] S. Schweidler, et al., J. Phys. Chem. C 122 (2018) 8829–8835, http://dx.doi.org/10.1021/acs.jpcc.8b01873.
[66] Y. Kuai, et al., Appl. Surf. Sci. 586 (2022) 152510, http://dx.doi.org/10.1016/j.apsusc.2022.152510.
[67] M.K. Masood, et al., J. Phys. Chem. Solids 186 (2023) 111814, http://dx.doi.org/10.1016/j.jpcs.2023.111814.
[68] Y. Wang, et al., J. Mater. Chem. A 8 (2020) 4274–4282, http://dx.doi.org/10.1039/C9TA11589G.
[69] X. Lv, et al., Phys. Chem. Chem. Phys. 2 (2020) 8902–8912, http://dx.doi.org/10.1039/D0CP00967A.
[70] P. Patel, et al., ACS Appl. Nano Mater. 6 (2023) 2103–2115, http://dx.doi.org/10.1021/acsanm.2c05090.
[71] D. Chodvadiya, et al., Appl. Surf. Sci. 593 (2012) 153424, http://dx.doi.org/10.1016/j.apsusc.2022.153424.
[72] Y. Yu, et al., J. Mater. Chem. A 7 (2019) 12145–12153, http://dx.doi.org/10.1039/C9TA02650A.
[73] Y. Jing, et al., J. Phys. Chem. C 117 (2013) 25409–25413, http://dx.doi.org/10.1021/jp410969.
[74] S. Zhao, et al., J. Mater. Chem. A 2 (2014) 19046–19052, http://dx.doi.org/10.1039/C4TA04368E.
[75] B. Mortazavi, et al., Electrochim. Acta 213 (2016) 865–870, http://dx.doi.org/10.1016/j.electacta.2016.08.027.
[76] G. Barik, et al., J. Phys. Chem. C 123 (2019) 21852–21865, http://dx.doi.org/10.1021/acs.jpcc.9b04128.
[77] J. Deb, et al., ACS Appl. Nano Mater. 2 (2022) 10572–10582, http://dx.doi.org/10.1021/acsanm.2c01909.
[78] P. Patel, et al., J. Energy Storage 71 (2023) 108074, http://dx.doi.org/10.1016/j.est.2023.108074.
[79] W.C. Sun, et al., J. Mater. Sci. 56 (2021) 13763–13771, http://dx.doi.org/10.1007/s10853-021-06174-9.
[80] Z. Tabandeh, et al., J. Energy Storage 76 (2024) 109640, http://dx.doi.org/10.1016/j.est.2023.109640.
[81] Z. Wang, et al., Appl. Surf. Sci. 593 (2022) 153354, http://dx.doi.org/10.1016/j.apsusc.2022.153354.
[82] J. Park, et al., Appl. Surf. Sci. 638 (2023) 158024, http://dx.doi.org/10.1016/j.apsusc.2023.158024.
[83] H. Lin, et al., Appl. Surf. Sci. 544 (2021) 148895, http://dx.doi.org/10.1016/j.apsusc.2020.148895.
[84] H. Jafari, et al., Solid State Commun. 282 (2018) 21–27, http://dx.doi.org/10.1016/j.ssc.2018.07.010.
[85] M. Parrinello, et al., Phys. Rev. Lett. 45 (1980) 1196, http://dx.doi.org/10.1103/PhysRevLett.45.1196.
[86] F. Mouhat, F.X. Coudert, Phys. Rev. B 90 (2014) 224104, http://dx.doi.org/10.1103/PhysRevB.90.224104.
[87] Y. Zhang, et al., J. Phys. Chem. Lett. 10 (2019) 6656–6663, http://dx.doi.org/10.1021/acs.jpclett.9b02599.
[88] R.C. Andrew, et al., Phys. Rev. B 85 (2012) 125428, http://dx.doi.org/10.1103/PhysRevB.85.125428.